

Hydrogen diffusivity and electrical anisotropy of a peridotite mantle

Fiona Simpson¹ and Andréa Tommasi²

¹*Institut für Geophysik, Universität Göttingen, Germany. E-mail: Fiona.Simpson@geo.physik.uni-goettingen.de*

²*Laboratoire de Tectonophysique, CNRS and Université Montpellier II, France*

Accepted 2004 December 16. Received 2004 December 16; in original form 2003 November 14

SUMMARY

Long-period magnetotelluric (MT) data have indicated that electrical conductivity in the upper mantle is highly anisotropic. Rates and anisotropies for self-diffusion of hydrogen in single crystals of mantle minerals are related to electrical resistivity by the Nernst–Einstein relationship. Assuming that the dominant mechanism for electrical conduction in the mantle is hydrogen diffusion, the electrical anisotropy of a peridotite should be controlled by its mineral composition and by the lattice-preferred orientation (LPO) of its constitutive minerals. Macroscopic electrical anisotropies arising from diffusion of hydrogen in upper mantle rocks displaying strain-induced LPO of olivine, enstatite and diopside are calculated using resistor networks in which each resistor has a statistical probability of representing a mineral grain with a particular misorientation relative to the olivine [100] maximum density direction. The orientations of the grains are defined by angular distribution functions describing LPO (1) generated by viscoplastic self-consistent modelling at a range of shear strains and (2) measured in a naturally deformed peridotite. The naturally deformed peridotite displays a strong LPO, but the predicted mean electrical anisotropy factor is less than 3. Geophysical data indicate higher electrical anisotropies for the mantle. This suggests that grain boundary processes that are controlled by shape-preferred orientation of crystals and/or macroscopic heterogeneities further enhance the electrical anisotropy of the mantle. Ambiguities in the conduction mechanism highlight the need for direct laboratory measurements of ionic conductivities in mantle assemblages that can be compared with those calculated from the Nernst–Einstein equation.

Key words: deformation, electrical conductivity, hydrogen diffusivity, lattice-preferred orientation, mantle anisotropy, olivine.

1 INTRODUCTION

Although mantle minerals are nominally anhydrous, they are able to incorporate dissociated H⁺ and OH⁻ ions (Mackwell & Kohlstedt 1990; Bell & Rossman 1992). Measured concentrations of hydrogen content in natural samples indicate that pyroxene minerals are the most important reservoirs for hydrogen in the upper mantle, followed by garnet and olivine (Bell & Rossman 1992).

Hydrogen diffusion in the mantle could enhance the electrical conductivity of the mantle according to the Nernst–Einstein equation (Karato 1990):

$$\sigma = f D c q^2 / k T \quad (1)$$

where σ is the electrical conductivity, f is a numerical (correlation) factor approximately equal to unity, D is the diffusivity, c is the concentration of diffusing ions, q is the electrical charge of the charged species, k is the Boltzmann constant and T is the temperature. Hydrogen diffusivities vary depending on mineral phase, and they may be strongly anisotropic. For example, hydrogen diffuses along the [100] axis of olivine approximately 20 times faster than along the [010] axis and 40 times faster than along the [001] axis (Kohlstedt

& Mackwell 1998), whereas pure enstatite is isotropic with respect to hydrogen diffusivity (Stalder & Skogby 2003) and has diffusion rates approximately 500 times slower than olivine. Hydrogen diffusivity rates in upper mantle minerals relative to diffusivities in olivine along the [100] direction are shown in Table 1.

If minerals are preferentially oriented in the mantle, then anisotropic rates of hydrogen diffusion should enhance the electrical conductivity of the mantle in one direction more than in other directions (Lizzaralde *et al.* 1995), i.e. the mantle can be expected to be electrically anisotropic. Evidence for strain-induced, lattice-preferred orientation (LPO) of minerals in the mantle, in particular of olivine, which is the dominant phase in the upper mantle, derives from analysis of naturally deformed peridotites (e.g. Nicolas & Christensen 1987), from laboratory experiments on olivine aggregates (Nicolas *et al.* 1973; Zhang & Karato 1995; Bystricky *et al.* 2000) and polycrystal plasticity models (Wenk *et al.* 1991; Tommasi *et al.* 2000; Kaminski & Ribe 2001). Moreover, seismic anisotropy data indicate that olivine LPO is coherent over large distances (from tens to hundreds of kilometres) in the upper mantle (Montagner & Tanimoto 1991). However, because alignment of minerals in the mantle is imperfect, the degree of electrical anisotropy that results

Table 1. Relative hydrogen diffusion rates along the main crystallographic axes of olivine (Kohlstedt & Mackwell 1998), pure enstatite (Stalder & Skogby 2003), Mg-rich orthopyroxene (Stalder & Skogby 2003) and diopside (Woods *et al.* 2000) at 700–900 °C.

	Olivine	Enstatite	Orthopyroxene	Diopside
[100]	500	1	6	750
[010]	25	1	1.9	50
[001]	12.5	1	15	—

from anisotropic rates of hydrogen diffusion can be expected to be reduced compared with the anisotropic hydrogen diffusion rates for the single crystals shown in Table 1.

The aim of this paper is to quantify the degree of electrical anisotropy that can be expected to arise in a peridotite mantle as a consequence of hydrogen diffusivity in nominally anhydrous mantle minerals (NAMS) combined with the strain-dependent LPO of these minerals that is induced by plastic flow in the mantle. The results are compared with geophysical data from different tectonic environments that indicate electrical anisotropies of the mantle in the range ~ 2.5 to >100 (Simpson 2001; Bahr & Simpson 2002; Leibegger *et al.* 2002).

2 HYDROGEN DIFFUSIVITY, MEASUREMENT ERRORS AND ELECTRICAL ANISOTROPY OF OLIVINE

If a crystal has H^+ diffusivities that are anisotropic, then the contribution of the ionic conductivity within this crystal to its overall electrical conductivity will also be anisotropic and the contribution of this crystal to the electrical conductivity of the rock (crystal aggregate) measured in a particular direction will depend on the orientation of the crystal within the aggregate. The orientations of individual crystals within an aggregate may be described by an orientation distribution function (ODF) (Bunge 1982) which describes the LPO of the aggregate. Minerals contained in naturally deformed peridotites exhibit LPOs that agree well with LPOs modelled for a simple shear deformation using a viscoplastic self-consistent (VPSC) approach (Tommasi *et al.* 2000). In this paper, LPOs calculated for olivine–pyroxene aggregates deformed at a range of shear strains and H^+ diffusivity data are used to generate electrical anisotropy distribution functions. These electrical anisotropy distribution functions are subsequently used to simulate electrical anisotropy of olivine–pyroxene aggregates using resistor networks (Simpson 2002). A similar approach is employed to calculate the mean electrical anisotropy factor for a naturally deformed peridotite displaying a well-developed LPO.

Magnetotelluric (MT) data provide two mutually-independent values of conductivity in the horizontal plane (e.g. parallel and perpendicular to strike) from which conductivities in all other directions in the plane can be calculated. Vertical electrical anisotropy (i.e. horizontal layering) cannot be resolved using MT measurements. Therefore it is sufficient to calculate the electrical conductivities arising from hydrogen diffusivity in the horizontal plane in order to quantify the contribution of a strain-induced LPO to the electrical anisotropy detected in MT data. The 2-D modelling procedure employed in this paper is summarized in Fig. 1, and involves the following sequence of steps:

(1) Step 1 involves defining the orientation of the individual grains composing the aggregate. The LPO are obtained ei-

ther by VPSC modelling at a range of shear strains (Tommasi 1998; Tommasi *et al.* 2000) or from electron-backscattered diffraction (EBSD) measurements in a naturally deformed peridotite, and are tabulated as Bunge–Euler angles (Bunge 1982).

(2) Step 2 involves projecting the LPO from step 1, for a particular shear strain or deformed sample, onto pole figures. This allows the maximum density direction (MDD) for olivine [100] axes to be defined. If hydrogen diffusivity is the conduction mechanism responsible for electrical anisotropy of the mantle, then the direction of maximum conductivity should correspond to the MDD of olivine [100] axes ($MDD_{[100]}$), since hydrogen diffusivities in olivine are more anisotropic than in other minerals and olivine is the predominant mantle mineral (>60 per cent). Directions parallel and perpendicular to $MDD_{[100]}$ are used to define a reference coordinate frame in subsequent steps.

(3) In step 3, the contributions of each crystal to hydrogen diffusivities parallel and perpendicular to $MDD_{[100]}$ (obtained from step 2) are calculated using simple trigonometric relations that consider hydrogen diffusivities as vector quantities with magnitudes defined by $D[100]:D[010]:D[001]$ ratios and the crystal orientation relative to $MDD_{[100]}$.

(4) In step 4a the relative resistivity of each crystal in the horizontal (x – y coordinate) plane, parallel and perpendicular to $MDD_{[100]}$, is computed from its hydrogen diffusivities parallel and perpendicular to $MDD_{[100]}$ (from step 3). The ratio of the relative resistivity parallel to $MDD_{[100]}$ to the relative resistivity perpendicular to $MDD_{[100]}$ for a particular crystal defines the electrical anisotropy factor of the crystal in the x – y coordinate plane. Electrical anisotropy factors are calculated for each crystal and the number of occurrences of each particular anisotropy factor (step 4b) leads to a distribution function of single-crystal electrical anisotropy factors in the $MDD_{[100]}$ coordinate frame (step 4c). The example shown in step 4c assumes hydrogen diffusivities in the ratios $D[100] = 20 \times D[010] = 40 \times D[001]$, which we shall refer to as the ‘preferred’ hydrogen diffusivities for olivine (Kohlstedt & Mackwell 1998). The sample from which these single-crystal anisotropies were calculated has the well-defined LPO shown in step 2. In this case, olivine [100] and [001] axes lie closest to the horizontal plane, and maximum single-crystal electrical anisotropies of 40 are obtained. The mean single-crystal anisotropy is ~ 8 , and approximately 29 per cent of the 1000 crystals in the sample have electrical resistivities perpendicular to $MDD_{[100]}$ that are about 10 or more times higher than their electrical resistivities parallel to $MDD_{[100]}$.

(5) In step 5, the relative resistivities computed in step 4 are used to compute a probability distribution function that defines the probability that any (x , y) resistor pair in the resistor network model has a particular set of (ρ_x , ρ_y) values (i.e. the probability that a particular single-crystal anisotropy contributes to the aggregate). For an aggregate containing more than one mineral type, the volume fractions of the different minerals present in the aggregate is taken into account when calculating these probabilities.

(6) In step 6, each (x , y) resistor pair in a resistor network (with $n \times n$ resistors in the x -direction and $(n - 1) \times (n - 1)$ resistors in the y -direction) is randomly assigned a pair of ρ_x , ρ_y values with the probabilities computed in step 5. The experiment is repeated for 100 networks. Each network represents a statistical approximation of the LPO of the aggregate.

(7) In step 7, possible effects of different hydrogen concentrations in different NAMS can be investigated by decreasing or increasing the (ρ_x , ρ_y) at sites in the network depending on the mineral phase flagged and the relative hydrogen concentration recorded for this mineral type.

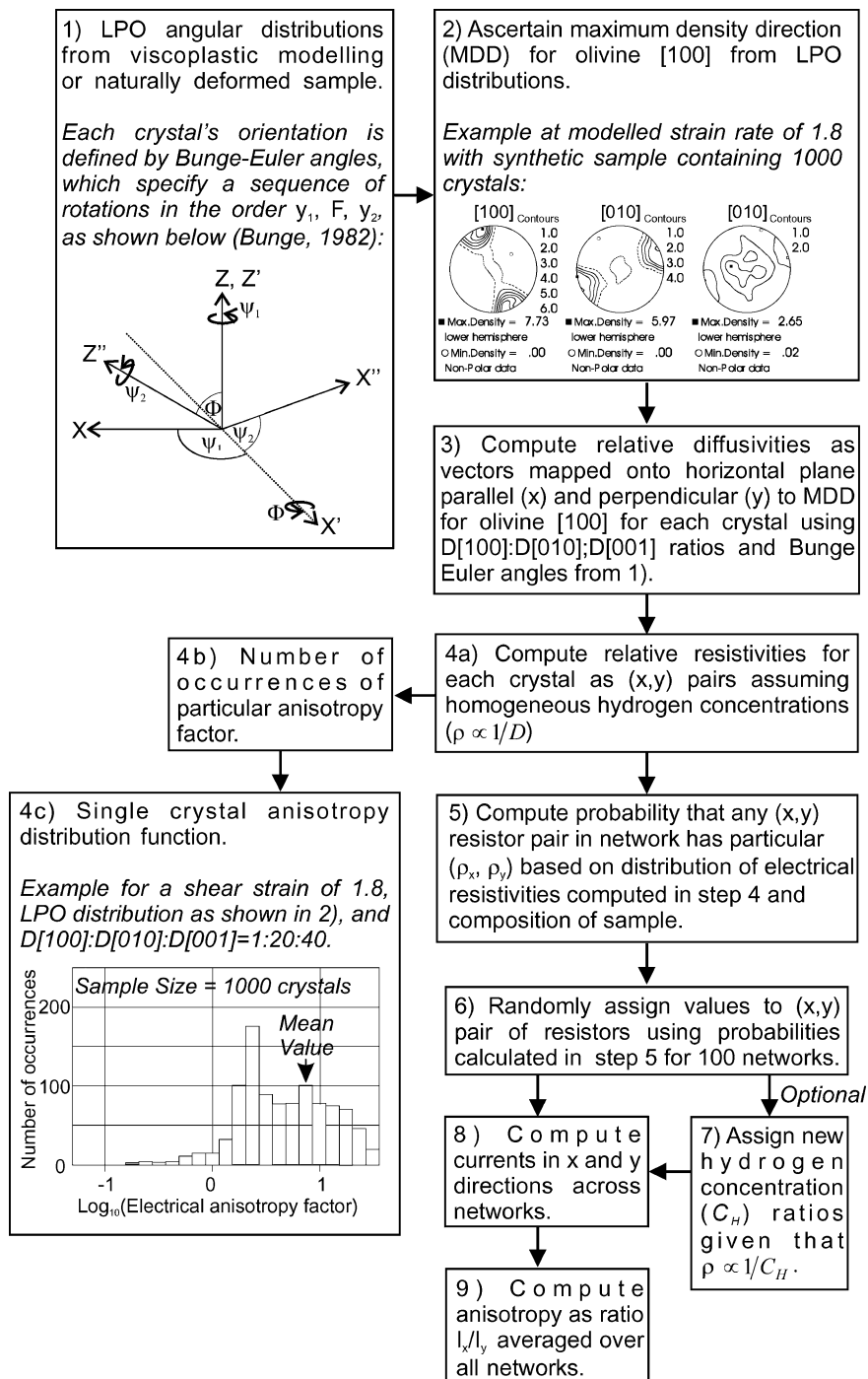


Figure 1. Flowchart illustrating the steps involved in calculating macroscopic electrical anisotropy factors from a network of resistors representing a mantle rock with an LPO of its constitutive minerals in which hydrogen diffusivities anisotropically enhance electrical conductivity, as given by the Nernst–Einstein equation.

(8) In step 8, voltages are applied across the resistor networks generated in step 6 (or step 7) in the x - and y -directions, respectively, and electrical currents I_x and I_y are computed for the two orthogonal directions (Bahr 2000).

(9) Finally (step 9), the electrical anisotropy of a random network is calculated as I_x/I_y .

Measurements of hydrogen diffusivities in olivine indicate best-fit values with ratios of $D[100] = 20 \times D[010] = 40 \times D[001]$

(Kohlstedt & Mackwell 1998). However, consideration of experimental errors suggests bounds ranging from $D[100] = 100 \times D[010] = 100 \times D[001]$ to $D[100] = 10 \times D[010] = 10 \times D[001]$. Bounds on the mean macroscopic electrical anisotropy factors as a function of shear strain for geodynamically modelled olivine LPO (Tommasi 1998) are shown in Fig. 2. The anisotropy is controlled primarily by hydrogen diffusion along the [100] and [001] axes, as for an asthenospheric flow associated with a velocity gradient between a tectonic plate and the deep mantle (Tommasi 1998); these

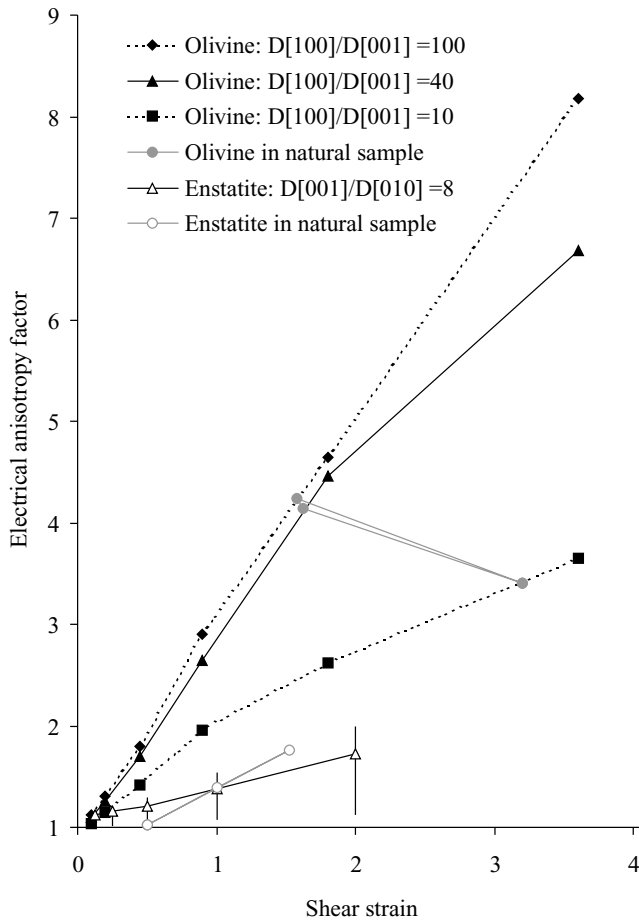


Figure 2. Bounds on the macroscopic electrical anisotropy factors (ratios of maximum to minimum conductivities) as a function of shear strain for aggregates composed of 100 per cent olivine (closed symbols) and 100 per cent enstatite (open symbols) assuming various single-crystal hydrogen diffusivities. For olivine, the preferred hydrogen diffusivity ratios $D[100] = 20 \times D[010] = 40 \times D[001]$ (Kohlstedt & Mackwell 1998) are assumed to be bounded by $D[100] = 100 \times D[010] = 100 \times D[001]$ and $D[100] = 10 \times D[010] = 10 \times D[001]$ respectively, whereas the error bars for the enstatite model represent ± 0.3 log unit uncertainties in hydrogen diffusivities (Stalder & Skogby 2003). Olivine and enstatite LPO were calculated for a 70 per cent olivine–30 per cent enstatite aggregate deformed by simple shear using a VPSC model. Grey circles indicate the shear strains at which the electrical anisotropy factors for 100 per cent olivine (closed) and orthopyroxene (open) aggregates displaying the LPO measured in a naturally deformed peridotite shown in Fig. 7 intersect the shear strain–electrical anisotropy bounds calculated from the synthetic aggregates. All results represent averages for 100 resistor networks with $n = 20$.

axes lie closest to the horizontal plane. The modelled electrical anisotropy for a 100 per cent olivine aggregate increases monotonically with increasing strain, reaching a factor of 8 at a shear strain of 3.5. The reduction in the electrical anisotropy from the single-crystal to aggregate scale is attributable to the dispersion of the olivine LPO. Although there is a factor of 10 difference between the upper and lower bound diffusivities along the [001] axes of an olivine crystal, the anisotropy of the aggregate calculated using different single-crystal anisotropies varies by a factor of only ~ 1.5 at a shear strain of 1 and ~ 1.8 at a shear strain of 2. Thus uncertainties in the measured hydrogen diffusivities are mapped into both x - and y -resistivity components. This implies that uncertainties as-

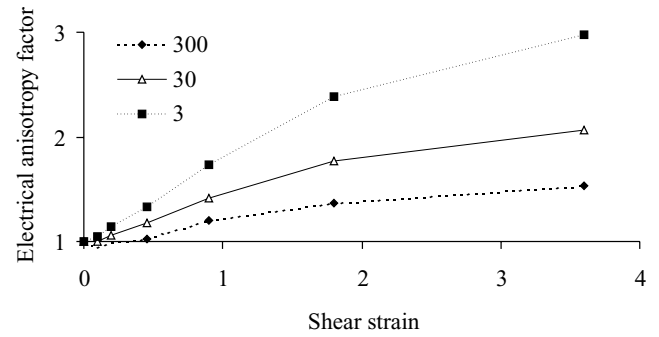


Figure 3. Macroscopic electrical anisotropy factor as a function of shear strain for a rock composed of 65 per cent olivine with LPO intensities developed by simple shear, and 35 per cent isotropic component. A single crystal of olivine is assumed to have $\sigma_{[100]} = 20 \times \sigma_{[010]} = 40 \times \sigma_{[001]}$, where $\sigma_{[100]}$, $\sigma_{[010]}$ and $\sigma_{[001]}$ are the relative conductivities of the [100], [010] and [001] axes, respectively. The isotropic phase has a conductivity 300, 30 or 3 times less than the conductivity along the olivine [100] axis.

sociated with measuring hydrogen diffusivities are unlikely to affect macroscopic electrical anisotropy factors significantly.

3 THE EFFECT OF ENSTATITE ON ELECTRICAL ANISOTROPY

If a second mineral phase with isotropic hydrogen diffusivities is mixed with olivine, the reduction in the macroscopic electrical anisotropy factor will depend on the hydrogen diffusivities of this mineral phase. This is demonstrated in Fig. 3, assuming that the hydrogen concentration is the same in both mineral phases.

The presence of enstatite as a second mineral phase does not modify olivine LPO patterns (Wenk *et al.* 1991). Hence, the effect of incorporating enstatite into the model aggregate will depend on the volume fraction of enstatite and on the conduction mechanism that is dominant in enstatite. Measurements of the electrical conductivity of dry orthopyroxene by Duba *et al.* (1973) and Xu & Shankland (1999) suggest electrical conductivities in the same range as those for dry olivine (Duba *et al.* 1974; Hirsch *et al.* 1993; Xu *et al.* 1998), i.e. significantly lower than those associated with H^+ conduction in olivine. Hydrogen diffusivities in pure enstatite are isotropic and approximately 500 times slower than those along olivine [100] (Stalder & Skogby 2003). The effects of incorporating 35 per cent and 22 per cent pure enstatite into the olivine model assuming hydrogen diffusion to be the controlling conduction mechanism are shown in Fig. 4. In this case, the low hydrogen diffusivities in enstatite relative to olivine and the volume fraction of enstatite in the aggregate control the degree to which the electrical anisotropy of an olivine–enstatite aggregate is altered compared with the electrical anisotropy obtained for the 100 per cent olivine model. The composition of the aggregate has a much more significant effect on the macroscopic electrical anisotropy than do uncertainties in the hydrogen diffusion rates in olivine.

On the other hand, more recent electrical conductivity data for dry orthopyroxene (Xu *et al.* 2000) are approximately 1.3 log units higher than those measured by Duba *et al.* (1973) and Xu & Shankland (1999). The measurements were performed at similar oxygen fugacities, and Xu *et al.* (2000) attribute the higher electrical conductivity of their sample to a higher ferric iron content. In this case, the conductivity of dry enstatite approaches the electrical conductivity controlled by hydrogen diffusivity in olivine with $1000 H/10^6 Si$. Considering the low rates of hydrogen diffusion in enstatite,

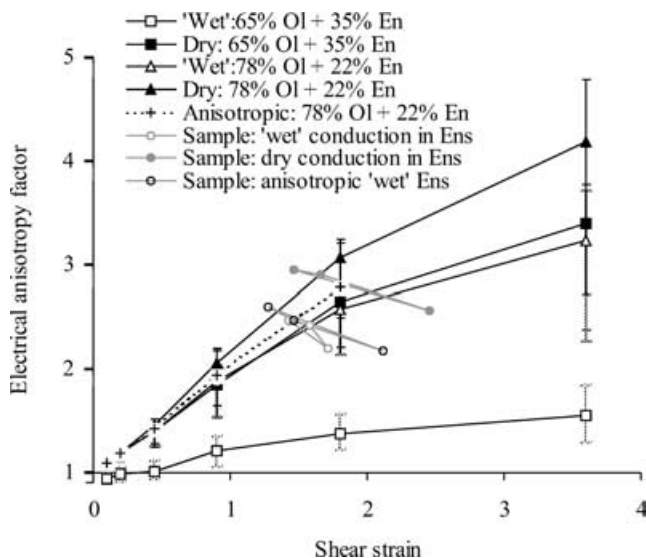


Figure 4. Average macroscopic electrical anisotropy factors as a function of shear strain for different olivine (Ol):enstatite (En) ratios and different conduction mechanisms in enstatite. For the ‘wet’ case, hydrogen diffusion in enstatite is approximately 500 times slower than along the olivine [100] axis; for the dry case, enstatite is assumed to have the same conductivity as the olivine [100] axis. The anisotropic case refers to the hydrogen diffusivities in orthopyroxene shown in Table 1. Hydrogen diffusivities in olivine are those given in Table 1 for all three cases. Error bars are based on upper and lower bounds for hydrogen diffusion in olivine defined by $D[100] = 100 \times D[010] = 100 \times D[001]$ and $D[100] = 10 \times D[010] = 10 \times D[001]$ respectively, combined with ± 0.3 log unit uncertainties in hydrogen diffusivities for enstatite. The hydrogen concentration is assumed to be the same in olivine and enstatite phases. ‘Sample’ refers to a model displaying the LPO of the naturally deformed sample shown in Fig. 7 with an Ol:En ratio of 78 per cent:22 per cent. Circles indicate the shear strains at which the electrical anisotropy factors calculated for the naturally deformed sample intersect the shear strain–electrical anisotropy bounds calculated from the aggregates synthesized by VPSC modelling. The enstatite component reduces the macroscopic anisotropy of the olivine–enstatite aggregates compared with olivine aggregates by reducing the connectivity of olivine [100] axes in the direction of maximum conductivity. The effect is least pronounced for the case that dry conduction in enstatite dominates. All results represent averages for 100 resistor networks with $n = 20$.

dry conduction may be the dominant conduction mechanism in enstatite. The effects of incorporating 35 per cent and 22 per cent enstatite into the model assuming that electrical conduction in enstatite is dominated by the dry conduction mechanism are also shown in Fig. 4. In this case the mean electrical anisotropy factor is raised compared with the case for slow hydrogen diffusivities in enstatite. This is because the conductive enstatite provides missing bridges for nearly through-going conductive pathways in the direction of olivine [100] alignment, whereas in the perpendicular direction, which contains more resistive elements, the fraction of conductive enstatite is insufficient to facilitate a significant increase in contiguity of conductive pathways (Fig. 5).

Hydrogen diffusivities in natural orthopyroxene ($\text{En}_{90}\text{Fs}_{10}$) are anisotropic: the [001] axis is the fastest direction, followed by [100] and [010]; the [001] axis is about eight times faster than the [010] axis (Stalder & Skogby 2003), and hydrogen diffusivities in natural orthopyroxene are one to two orders of magnitude slower than in olivine at 700 °C (Table 1). Mean macroscopic anisotropies for an orthopyroxene aggregate displaying a simple shear LPO averaged over 100 networks are shown in Fig. 2. The enstatite fast axis orients

approximately parallel to olivine [100], but has hydrogen diffusivities approximately equal to the slowest, [001], axis of olivine.

In contrast to crustal studies (Bahr 1997), in which resistivities may vary over 10 orders of magnitude, no significant systematic scale-dependence of electrical anisotropy arising from hydrogen diffusivity in the mantle is expected. This can be demonstrated by comparing the electrical anisotropies resulting from different sized networks (Fig. 6). The variation in mean electrical anisotropy for networks with values of n ranging from 10–40 does not exceed 20 per cent.

4 ELECTRICAL ANISOTROPY AS A CONSEQUENCE OF HYDROGEN DIFFUSIVITY IN A NATURALLY DEFORMED PERIDOTITE

Fig. 7 shows LPO distributions for a naturally deformed peridotite xenolith from a basaltic flow in the Fataua Valley, Tahiti. This spinel–herzolite (73 per cent olivine, 21 per cent enstatite, 5 per cent diopside and 1 per cent spinel) exhibits a coarse-grained porphyroclastic microstructure indicative of deformation under high-temperature, low-stress conditions, consistent with asthenospheric deformation. Relative hydrogen diffusivities along the main crystallographic axes of its constituent minerals are summarized in Table 1. Hydrogen diffusion rates in diopside at 700–800 °C are anisotropic with fastest transport along the [100] axis and slowest transport along the [010] axis, and are similar in magnitude to diffusion rates in olivine (Woods *et al.* 2000). Single-crystal anisotropy factors in the direction of olivine [100] maximum density are shown in Fig. 8. When only the olivine component is considered, with $D[100] = 20 \times D[010] = 40 \times D[001]$, the mean macroscopic anisotropy factor for the network is ~ 4 . This corresponds to the mean macroscopic anisotropies computed from modelled LPO intensities at a shear strain of 1.5–3 (Fig. 2). Taking into account the enstatite contribution (Fig. 7) reduces the mean macroscopic electrical anisotropy to < 3 (Fig. 4). The reduction is least for the case of dry conduction in enstatite and greatest if conduction in enstatite is assumed to be controlled by low, isotropic, hydrogen diffusivities. The diopside component has an insignificant effect on the electrical anisotropy of the naturally deformed sample (Table 2). The mean electrical anisotropy factor averaged over 100 networks generated by hydrogen diffusivity in the deformed peridotite is < 3 (Table 2). Comparison with Fig. 4 suggests that these results are compatible with deformation at a shear strain of 1.5–2.

Measurements of the hydrogen content of natural minerals indicate that orthopyroxenes have hydrogen concentrations on average 5.5 times higher than olivine, whilst diopside stores on average 12 times more hydrogen than olivine (Bell & Rossman 1992). According to the Nernst–Einstein equation (eq. 1), heterogeneous hydrogen concentrations should result in modified resistivities. However, the mean electrical anisotropy of the networks is not significantly affected (Table 2).

The naturally deformed peridotite contains no garnet. Hydrogen diffusivities in garnet are between one and three times those along the olivine [001] axis (Wang *et al.* 1996), but observations from naturally deformed rocks and VPSC simulations show that garnet LPO is always very weak (Mainprice *et al.* 2004). Thus a pyrolite mantle composed of approximately 60 per cent olivine, 10 per cent orthopyroxene, 15 per cent clinopyroxene and 15 per cent garnet (Ita & Stixrude 1992), which displays olivine LPOs similar to those of the naturally deformed peridotite shown in Fig. 7, and the hydrogen

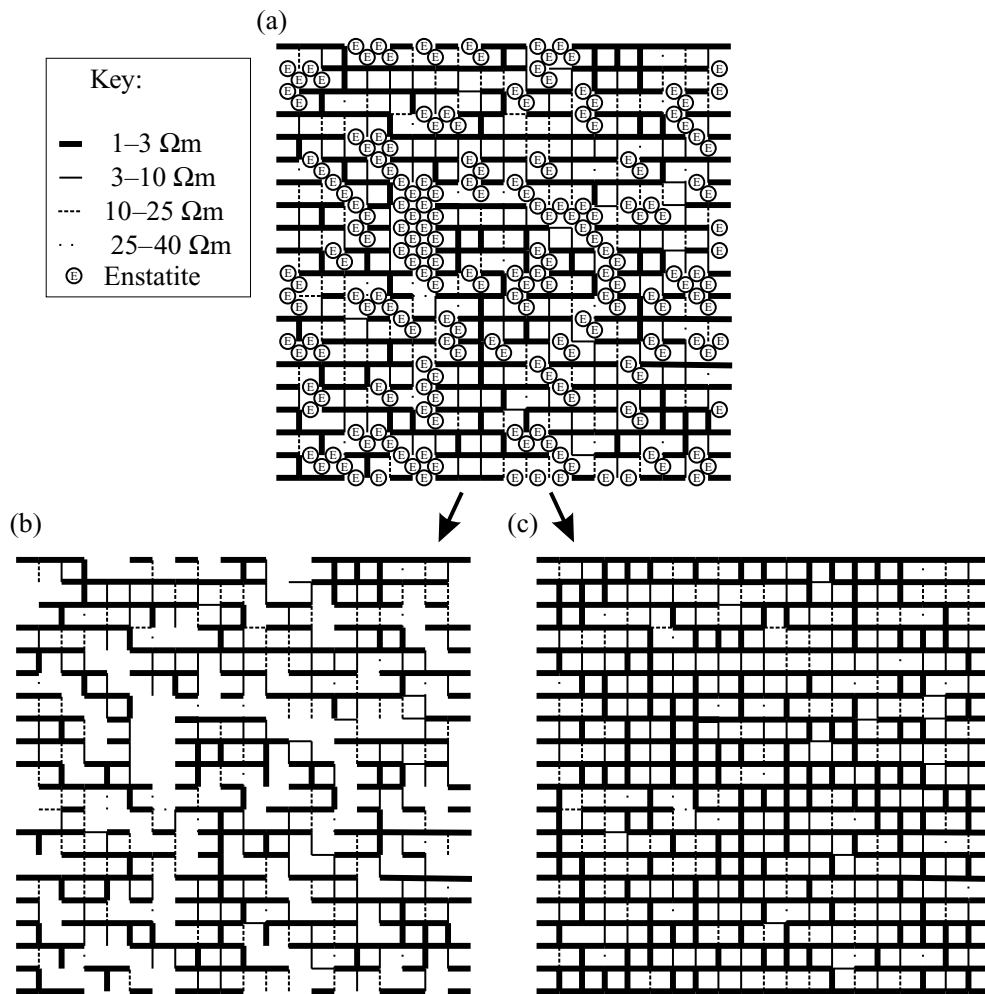


Figure 5. (a) Simplified resistor network composed of 78 per cent olivine and 22 per cent enstatite representing a realization of the LPO generated by VPSC modelling at a shear strain of 1.8. (b) The network for an exaggerated case (for visualization purposes only) in which the resistivity of enstatite is so high that it acts as a break in the circuit. (c) The network for the case that enstatite has the same resistivity as olivine along the [100] axis. The contiguity of conductive pathways differs for the two models.

diffusivities given in Table 1, will show a mean electrical conductivity anisotropy of <3 . Olivine LPO intensity does not increase linearly with strain, it increases fast at low strains up to 1 or 2, and it tends to remain stable for shear strains higher than 2–3 (Bystricky *et al.* 1999; Tommasi *et al.* 2000). So higher shear strains will not induce higher average electrical anisotropies.

However, electrical anisotropy factors for individual networks are spread over one to two orders of magnitude for the case in which hydrogen diffusivity controls conductivity of enstatite and about 0.5 orders of magnitude for the case in which the conductivity of enstatite is dominated by dry conduction (Fig. 9a). Based on the preferred hydrogen diffusivities in Table 1, the largest anisotropy factor generated by an individual resistor network representing a statistical realization of sample OED (Table 2) is ~ 14 ; 2 per cent of networks generate electrical anisotropy factors >10 ; 9 per cent of networks generate electrical anisotropy factors >5 . For the case in which conduction in enstatite is dominated by the dry conduction mechanism, the electrical anisotropy factor does not exceed 4 for any of the 100 networks. When upper and lower bounds for hydrogen diffusivities are taken into account (Fig. 9b), 95 per cent of the networks representing statistical realizations of the LPO of the naturally deformed sample have values in the range 0.8–8. The mean

electrical anisotropy factors calculated by averaging the results for 1000 networks do not differ significantly from those calculated by averaging the results from 100 networks (Table 2). Physically, electrical anisotropy factors less than 1 (Fig. 9) signify that the direction of maximum conductivity is perpendicular to the direction in which olivine [100] axes are statistically aligned. Electrical anisotropy factors less than 1 do not occur for the case that conduction in enstatite is dominated by the dry conduction mechanism.

5 COMPARISON OF EXPECTED ELECTRICAL ANISOTROPY FACTORS GENERATED BY HYDROGEN DIFFUSIVITY IN A PERIDOTITE MANTLE AND ELECTROMAGNETIC FIELD STUDIES

Long-period MT data indicate electrical anisotropies near the base of the lithospheric mantle below central Australia, northern Germany and Fennoscandia of >2 , >9 and >100 , respectively (Bahr & Simpson 2002). The Australian Plate has been moving at 6–7 cm yr⁻¹ in its present direction for ~ 40 Myr, which is compatible

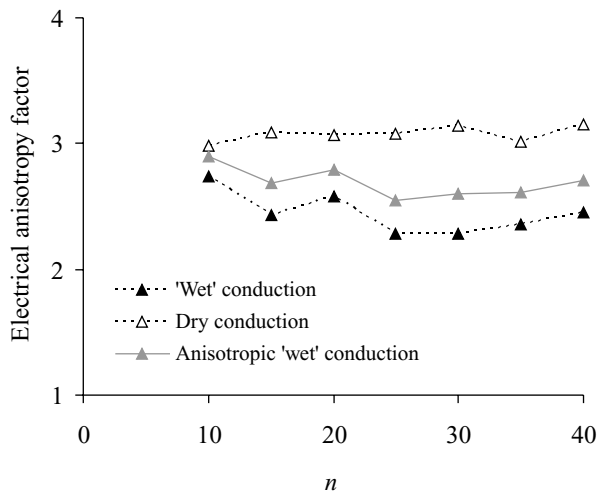


Figure 6. Macroscopic electrical anisotropy factors for different sized networks composed of $n \times n$ resistors in the x -direction and $(n - 1) \times (n - 1)$ resistors in the y -direction. The resistors represent an aggregate composed of 78 per cent olivine and 22 per cent enstatite with LPO for a shear strain of 1.8–2.0. ‘Wet’, ‘dry’ and anisotropic ‘wet’ conduction refer to the dominant conduction mechanism in enstatite. The dominant conduction mechanism in olivine is assumed to be hydrogen diffusivity in all cases. Each data point represents an average value calculated from 100 resistor networks. No systematic scale dependence of electrical anisotropy is apparent.

with a shear strain of 1–2. Therefore the olivine LPO intensity under central Australia could be reasonably assumed to be similar to that displayed by the naturally deformed peridotite shown in Fig. 7. In this case, a conduction mechanism that is dominated by anisotropic hydrogen diffusion rates in olivine can generate macroscopic electrical anisotropies of the same order of magnitude as those inferred from 1-D analysis of MT data containing anisotropy. The electrical anisotropies of the mantle below Fennoscandia are significantly higher than those expected to be generated by anisotropic rates of hydrogen diffusion. Bahr & Simpson (2002) note that some lateral variation of the conductance is evident in the data from Fennoscandia, and lateral conductivity heterogeneities may elevate the electrical anisotropy factors that are estimated from these data above their true values.

6 OTHER MECHANISMS FOR INCREASING THE ELECTRICAL ANISOTROPY OF THE MANTLE

Studies of melt migration in the Oman ophiolite complex demonstrate that focused migration of basaltic melt through harzburgite (olivine and enstatite) results in the formation of dunite (olivine only) conduits with widths ranging from the centimetre scale to up to 100 m (Braun & Kelemen 2002). Bands of dunite 30–100 cm wide with spacings of 10–100 m within a predominantly harzburgite

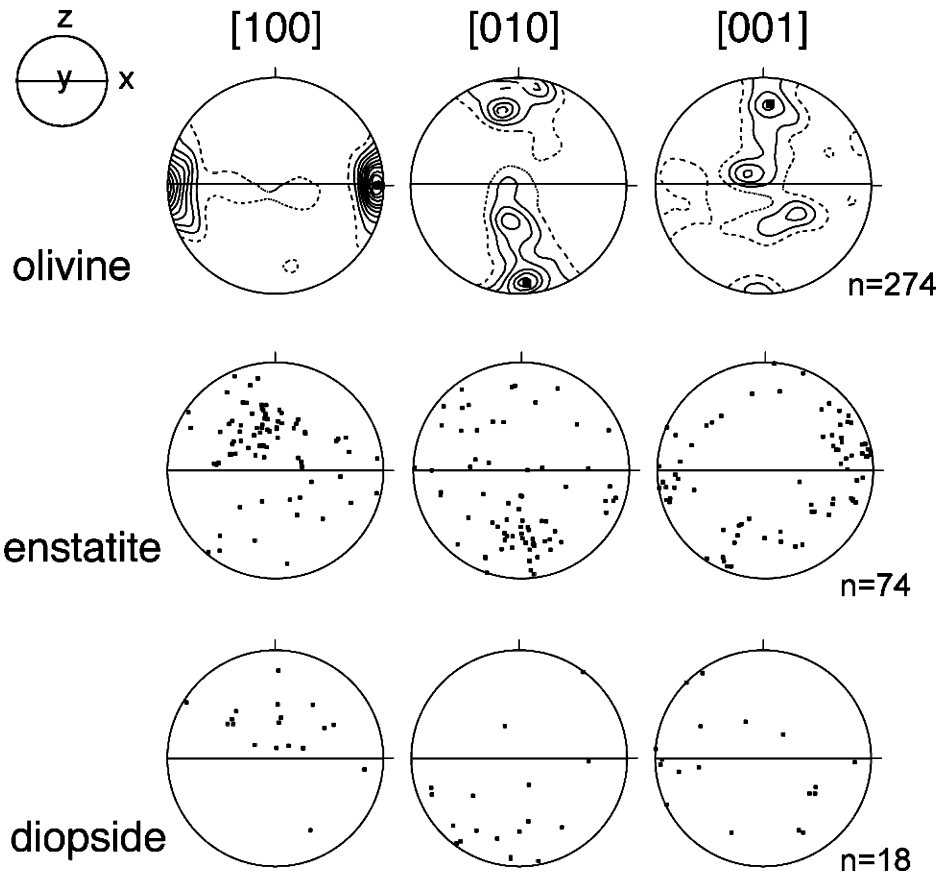


Figure 7. Olivine, enstatite and diopside LPO in a naturally deformed lherzolite: lower hemisphere equal-area projection, n grains. Olivine LPO was contoured at one multiple of a uniform distribution of intervals. Enstatite and diopside LPO were not contoured because fewer than 100 measurements were obtained in thin section. The full line marks the orientation of the foliation (XY plane); lineation (X direction) is horizontal.

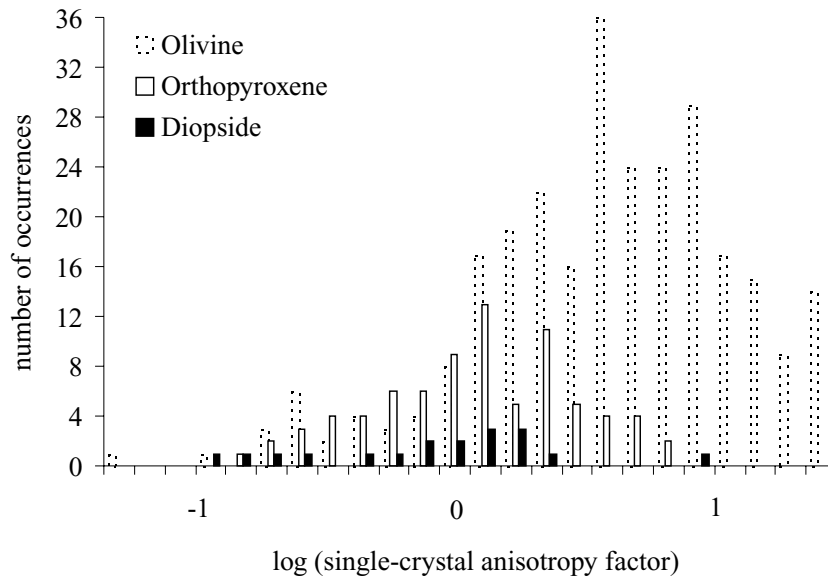


Figure 8. Distribution functions for the \log_{10} single-crystal electrical anisotropy factors relative to the olivine [100] maximum density direction calculated from the anisotropic hydrogen diffusivities shown in Table 1, based on the LPO distributions shown in Fig. 7.

Table 2. Average electrical anisotropy factors calculated from 100 and 1000 (in brackets) resistor networks representing a naturally deformed peridotite with the LPO and single-crystal electrical anisotropy factors shown in Figs 7 and 8 respectively. ‘Pure enstatite’ refers to the isotropic hydrogen diffusivities for enstatite given in Table 1, whereas ‘orthopyroxene’ refers to the anisotropic diffusion rates for Mg-rich orthopyroxene given in Table 1. The aggregate containing 74 per cent olivine, 21 per cent orthopyroxene and 5 per cent diopside is referred to in the text as sample ‘OED’. Hydrogen concentrations are assumed to be the same in all mineral phases, apart from in the last row where the hydrogen concentrations (C_H) are in the ratios given. Errors represent ± 0.3 log unit uncertainties for measured hydrogen diffusion rates in enstatite (Stalder & Skogby 2003) and upper and lower bounds on hydrogen diffusion rates in olivine of $D[100] = 100 \times D[010] = 100 \times D[001]$ and $D[100] = 10 \times D[010] = 10 \times D[001]$, respectively.

Composition	Anisotropy factor
100 per cent olivine	$4.1 \pm_{0.7}^{0.1}$ ($4.1 \pm_{0.7}^{0.1}$)
74 per cent olivine, 21 per cent dry enstatite, 5 per cent diopside	$2.9 \pm_{0.4}^{0.1}$ ($2.8 \pm_{0.4}^{0.1}$)
74 per cent olivine, 21 per cent pure enstatite, 5 per cent diopside	$2.5 \pm_{0.3}^{0.1}$ ($2.3 \pm_{0.3}^{0.1}$)
74 per cent olivine, 21 per cent orthopyroxene, 5 per cent diopside (OED)	$2.5 \pm_{0.4}^{0.1}$ ($2.4 \pm_{0.3}^{0.1}$)
OED; $C_{H(\text{Olivine})}:C_{H(\text{Enstatite})}:C_{H(\text{Diopside})} = 1:5.5:12$	$2.6 \pm_{0.5}^{0.2}$ ($2.5 \pm_{0.4}^{0.2}$)

matrix (75 per cent olivine, 25 per cent enstatite) have also been documented in peridotite massifs in the Canadian cordillera, where they produce a compositional banding at the massif scale that is aligned parallel to the deformation fabric of the massif (Ross 1977; Tommasi *et al.*, in preparation). MT transfer functions are unable to resolve conductivity variations that have horizontal dimensions less than (or even up to several times) the depth at which they are imaged, i.e. macroscopic and microscopic electrical anisotropy cannot be distinguished. Hence, for the purposes of evaluating electrical anisotropies at mantle depths a model consisting of an alternating sequence of more and less resistive dykes is equivalent to a model containing intrinsic electrical anisotropy. Alternating bands composed of pure olivine and 50 per cent enstatite–50 per cent olivine can produce anisotropies of the order of 100 (Fig. 10) assuming that the conduction mechanism is controlled by hydrogen diffusion. In this case, the enstatite grains act as a high-resistivity phase that blocks current flow perpendicular to the direction in which olivine [100] axes are statistically aligned. For the case that conduction in enstatite is controlled by a high ferric iron content (‘dry conduction’; Xu *et al.* 2000) the effect of such structural lineaments is mitigated

(Fig. 10). A pre-requisite for the development of such a structural anisotropy is partial melting, implying that it should be restricted to active tectonic regions such as oceanic ridges, the mantle wedge above a subduction zone, or be associated with mantle plumes.

A second mechanism that could give rise to olivine–enstatite banding is mechanical segregation in high-strain regions. Centimetre-scale banding characterized by alternating pyroxene-poor, predominantly dunitic layers with pyroxene-rich bands is indeed a characteristic feature of the high-temperature deformation domains of both ophiolites and orogenic peridotite massifs (Nicolas *et al.* 1971, 1980). This small-scale compositional banding, resulting from mechanical segregation of weak (olivine) and strong (pyroxene) phases during plastic deformation, is restricted to high-strain regions. Therefore, it may not be a generalized feature but rather may affect only small volumes of the mantle. Moreover, the electrical anisotropy associated with this compositional banding can only be detected by MT measurements if the layering is vertical or steeply dipping, i.e. if the flow planes are vertical or steeply dipping. Horizontal shearing of the asthenosphere due to mechanical drag of a moving tectonic plate is expected to produce horizontal layering.

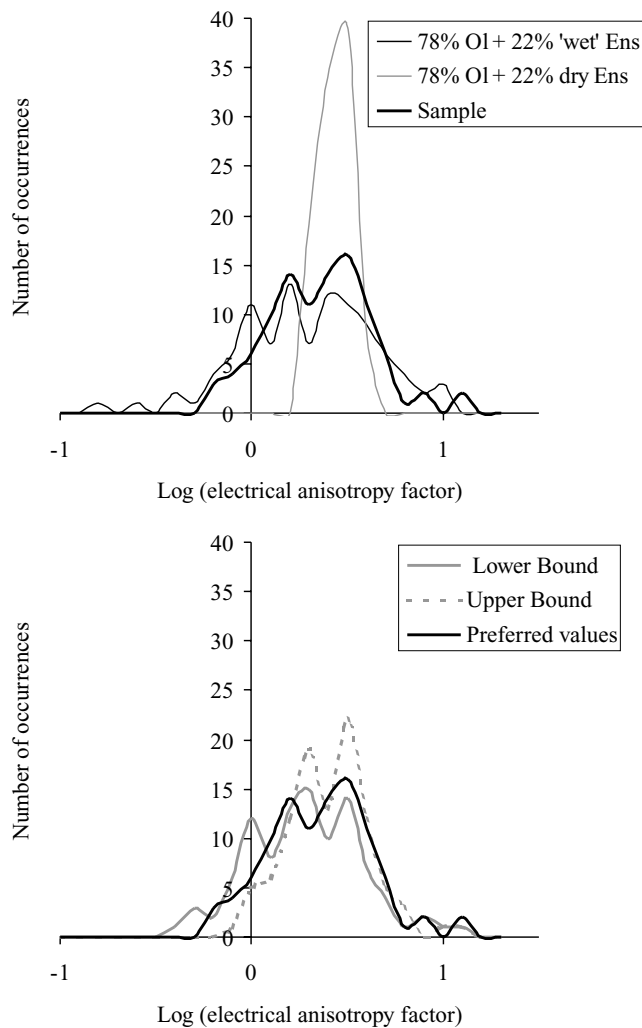


Figure 9. Distribution functions showing electrical anisotropy factors generated from 100 individual resistor networks with $n = 20$ and preferred hydrogen diffusivities shown in Table 1 for (a) a 78 per cent olivine plus 22 per cent enstatite composite with LPO predicted by VPSC modelling at a shear strain of 1.8 with either dry conduction or 'wet', isotropic conduction dominating in enstatite, and for sample OED (Table 2), and (b) preferred, upper and lower bound hydrogen diffusivities for sample OED.

Compositional banding arising from horizontal shearing should not contribute to the electrical anisotropy inferred from long-period MT data. However, compositional banding may be a factor enhancing the electrical anisotropy in the mantle beneath major transcurrent faults or transform plate boundaries, such as the Alpine Fault in New Zealand.

Shear strains associated with plate motion may favour shape-preferred orientation (SPO) as well as LPO of mantle minerals. Thus, in addition to hydrogen diffusion within olivine and other minerals displaying strong LPO, electrical anisotropy of the mantle may be enhanced by alignment of grain boundary phases (e.g. graphite, iron or partial melt). Graphite and iron are several orders of magnitude more conductive than olivine. Therefore grain-boundary graphite or iron could affect conductivity significantly. Shear stress has been shown (Ross & Bustin 1990) to lower the activation energy for graphitization under crustal conditions, and similar promotion of graphitization might happen during mantle shearing. Ando *et al.*

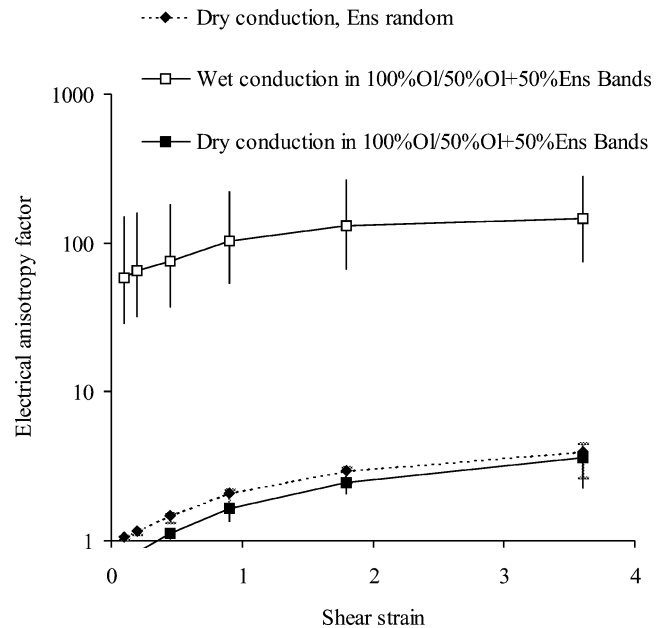


Figure 10. Average macroscopic electrical anisotropy factors for networks composed of resistors representing 75 per cent olivine (Ol) and 25 per cent enstatite (En) arranged to form alternating bands containing 100 per cent olivine versus 50 per cent olivine plus 50 per cent enstatite (Fig. 11) that create macroscopic anisotropy. Conduction in enstatite is assumed to be controlled by either slow, isotropic hydrogen diffusion rates ('wet' conduction) or by the dry conduction mechanism. For dry conduction in enstatite, the average electrical anisotropy is similar to the electrical anisotropy generated by a random distribution of enstatite. Results represent averages for 100 networks with $n = 20$.

(2001) have reported striped zoning of iron along subgrain boundaries of olivine in plastically deformed mantle peridotites.

Dry basaltic and andesitic melts are insufficiently electrically conductive (e.g. Tyburczy & Waff 1983; Roberts & Tyburczy 1999) to explain high mantle conductivities without inferring implausibly high melt fractions. However, faster hydrogen diffusion may take place in the melt phase. Hydrogen diffusion in the melt phase can be expected to be isotropic, but ionic conductivity can be expected to be anisotropic if the charge-carrying ions are anisotropically channelled. SPO of grain boundary melt in which hydrogen diffusion occurs could focus hydrogen diffusion along melt channels. Diffusion of other ions in the crystal and melt phases could also play a role. In diopside, the mobility of electron holes, rather than the mobility of hydrogen, is considered to be the phenomenon that controls the rate of hydrogen diffusion, and the mobility of electron holes has been found to be dependent on the Fe content of the sample (Hercule & Ingrin 1999).

Whereas electrical conductivity is a macroscopic quantity, self-diffusivity occurs in the $\text{mm}^2 \text{s}^{-1}$ range and may be modified by grain boundary effects. Equilibrium concentrations of hydrogen in mantle minerals depends on hydrogen fugacity and on the concentration of intrinsic point defects (Kohlstedt & Mackwell 1998); OH absorption spectra polarized along olivine [100], [010] and [001] indicate that OH defects are strongly oriented (Kitamura *et al.* 1987). If anisotropic diffusion rates for hydrogen in olivine arise from an anisotropic concentration of defects, then processes such as crystallographic alignment of defects and grain boundary diffusion in the mantle may lead to increased hydrogen-related electrical anisotropy in the mantle compared with that observed on the laboratory scale, and a modification of the Nernst–Einstein equation may also be

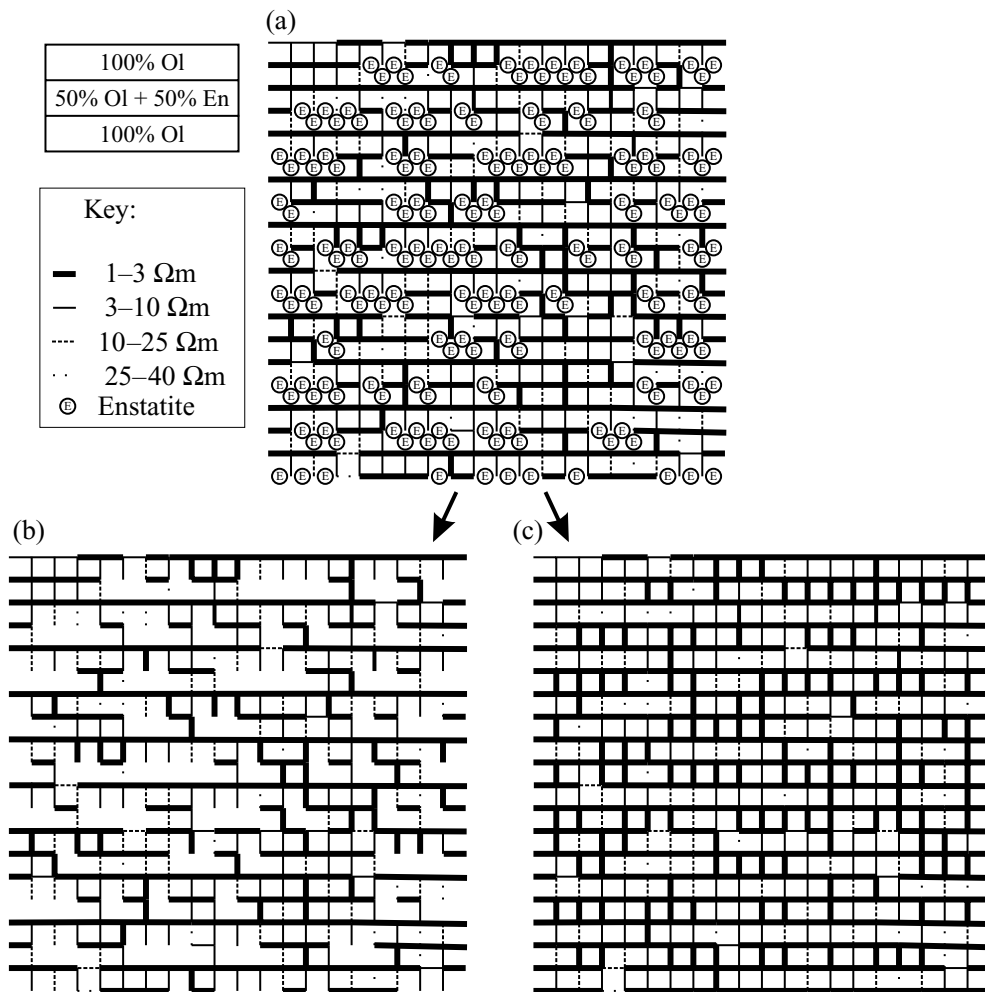


Figure 11. (a) Simplified example of a resistor network composed of 75 per cent olivine and 25 per cent enstatite contained in alternating bands of 100 per cent olivine and 50 per cent olivine plus 50 per cent enstatite with LPO intensities predicted by VPSC modelling at a shear strain of 1.8. (b) The network for an exaggerated case in which the resistivity of enstatite is so high that it acts as a break in the circuit. (c) The network for the case that enstatite has the same resistivity as the olivine [100] axis. Notice how the contiguity of conductive pathways differs for the models (b) and (c), and that (c) is similar to the model shown in Fig. 5(c).

required, as is the case for electrolyte gels (Fleischer *et al.* 1998). Grain boundary diffusion is likely to be quicker than lattice diffusion.

7 CONCLUSION

We have developed a model that allows the electrical anisotropy resulting from the coupled effects of anisotropic hydrogen diffusivity and LPO of mantle minerals to be quantified. The electrical anisotropy factors calculated using LPO simulated for olivine–enstatite aggregates deformed by simple shear are significantly less than the hydrogen-diffusion-related electrical anisotropy expected at the single-crystal scale. The mean electrical anisotropy factor (averaged over 100 or 1000 networks) generated by hydrogen diffusivity in a peridotite sample with well-developed LPO is <3 . Hence electrical anisotropy of the upper mantle below central Australia represents an upper limit on the mean degree of electrical anisotropy that can be generated by anisotropic hydrogen diffusion in a textured upper mantle. However, a spread of values to a maximum factor of 14 is obtained from 100 individual networks each representing a deformed sample in which hydrogen

diffusion is the dominant mechanism controlling conductivity. On the other hand, electrical anisotropy factors of less than 1 arising in a few networks suggest a statistical mechanism whereby maximum electrical conductivities may be produced oblique to the direction in which olivine [100] axes are expected to be statistically aligned.

To date, few MT array studies with sounding periods sufficiently long to resolve mantle anisotropy have been performed. Further MT array studies are required in order to quantify possible regional differences in mantle anisotropies, and to preclude multi-dimensional distortion of the electrical anisotropy factors obtained from field data. Ambiguities in the conduction mechanism highlight the need for laboratory measurements of electrical conductivity in NAMS under mantle conditions that can be compared with the electrical conductivities predicted by the Nernst–Einstein equation.

ACKNOWLEDGMENTS

Reviews by Greg Hirth and an anonymous reviewer helped to improve the paper. We also thank Martyn Unsworth (editor).

REFERENCES

- Ando, J., Shibata, Y., Okajima, Y., Kanagawa, K., Furusho, M. & Tomioka, N., 2001. Striped iron zoning of olivine induced by dislocation creep in deformed peridotites, *Nature*, **414**, 893–895.
- Bahr, K., 1997. Electrical anisotropy and conductivity distribution functions of fractal random networks and of the crust: the scale effect of connectivity, *Geophys. J. Int.*, **130**, 649–660.
- Bahr, K., 2000. Percolation in the crust derived from distortion of electric fields, *Geophys. Res. Lett.*, **27**, 1049–1052.
- Bahr, K. & Simpson, F., 2002. Electrical anisotropy below slow- and fast-moving plates: palaeoflow in the upper mantle?, *Science*, **295**, 1270–1272.
- Bell, D.R. & Rossman, G.R., 1992. Water in Earth's mantle: the role of nominally anhydrous minerals, *Science*, **255**, 1391–1397.
- Braun, M.G. & Kelemen, P.B., 2002. Dunite distribution in the Oman ophiolite: implications for melt flux through porous dunite conduits, *Geochem. Geophys. Geosyst.*, **3**(11), 8603, doi:10.1029/2001GC000289.
- Bunge, H.-J., 1982. *Texture Analysis in Materials Science*, p. 36, Butterworth, London.
- Bystricky, M., Burlini, L., Kunze, K. & Burg, J.P., 1999. Experimental deformation of olivine aggregates to high strains in torsion, *Göttinger Arb. Geol. Paläont.*, **Sb4**, (Texture and Physical Properties of Rocks), 22–23.
- Bystricky, M., Kunze, K., Burlini, L. & Burg, J.P., 2000. High shear strain of olivine aggregates; rheological and seismic consequences. *Science*, **290** (5496), 1564–1567.
- Duba, A., Boland, J.N. & Ringwood, A.E., 1973. The electrical conductivity of pyroxene, *J. Geol.*, **81**, 727–735.
- Duba, A., Heard, H.C. & Schock, R.N., 1974. Electrical conductivity of olivine at high pressure and under controlled oxygen fugacity, *J. geophys. Res.*, **79**, 1667–1673.
- Fleischer, G., Scheller, H., Kärger, J., Reiche, A. & Sandner, B., 1998. Correlation of self-diffusivity and ionic conductivity in gel electrolytes on basis of oligo(ethylene glycol)_n-dimethacrylate, *J. Non-cryst. Solids*, **235–237**, 742–747.
- Hercule, S. & Ingrin, J., 1999. Hydrogen in diopside: diffusion, extraction-incorporation, and solubility, *Am. Mineral.*, **84**, 1577–1588.
- Hirsch, L.M., Shankland, T. & Duba, A., 1993. Electrical conduction and polaron mobility in Fe-bearing olivine, *Geophys. J. Int.*, **114**, 36–44.
- Ita, J. & Stixrude, L., 1992. Petrology, elasticity and composition of the mantle transition zone, *J. geophys. Res.*, **97**, 6849–6866.
- Kaminski, E. & Ribe, N.M., 2001. A kinematic model for recrystallisation and texture development in olivine polycrystals, *Earth planet. Sci. Lett.*, **189**, 253–267.
- Karato, S.-I., 1990. The role of hydrogen in the electrical conductivity of the upper mantle, *Nature*, **347**, 272–273.
- Kitamura, M., Kondoh, S., Morimoto, N., Miller, G., Rossman, G.R. & Putnis, A., 1987. Planar OH-bearing defects in mantle olivine, *Nature*, **328**, 143–145.
- Kohlstedt, D. & Mackwell, S., 1998. Diffusion of hydrogen and intrinsic point defects in olivine, *Z. Phys. Chem.*, **207**, 147–162.
- Leibecker, J., Gatzemeier, A., Hönig, M., Kuras, O. & Soyer, W., 2002. Evidence of electrical anisotropic structures in the lower crust and the upper mantle beneath the Rhenish Shield, *Earth planet. Sci. Lett.*, **202**, 289–302.
- Lizzaralde, D., Chave, A., Hirth, G. & Schultz, A., 1995. Northeastern Pacific mantle conductivity profile from long period magnetotelluric sounding using Hawaii to California submarine cable data, *J. geophys. Res.*, **100**, 17 837–17 854.
- Mackwell, S.J. & Kohlstedt, D.L., 1990. Diffusion of hydrogen in olivine: implications for water in the mantle, *J. geophys. Res.*, **95**, 5079–5088.
- Mainprice, D., Bascou, J., Cordier, P. & Tommasi, A., 2004. Crystal preferred orientations of garnet: comparison between numerical simulations and electron-backscattered diffraction measurements in naturally deformed eclogites, *J. Struct. Geol.*, **26**, 2089–2102.
- Montagner, J.-P. & Tanimoto, T., 1991. Global upper mantle tomography of seismic velocities and anisotropies, *J. geophys. Res.*, **96**, 20 337–20 351.
- Nicolas, A. & Christensen, N.I., 1987. Formation of anisotropy in upper mantle peridotites—a review, in *Composition, Structure and Dynamics of the Lithosphere–Asthenosphere System*, AGU Geodynamics Series 16, pp. 111–123, eds Fuchs, K. & Froidevaux, C., American Geophysical Union, Washington, DC.
- Nicolas, A., Bouchez, J.L. & Boudier, F., 1971. Textures, structures and fabrics due to solid state flow in some European lherzolites, *Tectonophysics*, **12**, 55–86.
- Nicolas, A., Boudier, F. & Boullier, A.M., 1973. Mechanism of flow in naturally and experimentally deformed peridotites, *Am. J. Sci.*, **273**, 853–876.
- Nicolas, A., Boudier, F. & Mercier, J., 1980. Interpretation of peridotite structures from ophiolitic and oceanic environments, *Am. J. Sci.*, **280**, 192–210.
- Roberts, J.J. & Tyburczy, J.A., 1999. Partial-melt electrical conductivity: influence of melt-composition, *J. geophys. Res.*, **104**, 7055–7065.
- Ross, J.V., 1977. The internal fabric of an alpine peridotite near Pinchi Lake, central British Columbia, *Can. J. Earth Sci.*, **14**, 32–44.
- Ross, J.V. & Bustin, R.M., 1990. The role of strain energy in creep graphitisation of anthracite, *Nature*, **343**, 58–60.
- Simpson, F., 2001. Resistance to mantle flow inferred from the electromagnetic strike of the Australian upper mantle, *Nature*, **412**, 632–634.
- Simpson, F., 2002. Intensity and direction of lattice-preferred orientation of olivine: are electrical and seismic anisotropies of the Australian mantle reconcilable?, *Earth planet. Sci. Lett.*, **203**, 535–547.
- Stalder, R. & Skogby, H., 2003. Hydrogen diffusion in natural and synthetic orthopyroxene, *Phys. Chem. Miner.*, **30**, 12–19.
- Tommasi, A., 1998. Forward modelling of the development of seismic anisotropy in the upper mantle, *Earth planet. Sci. Lett.*, **160**, 1–13.
- Tommasi, A., Mainprice, D., Canova, G. & Chastel, Y., 2000. Viscoplastic self-consistent and equilibrium-based modelling of olivine lattice preferred orientations. Implications for upper mantle seismic anisotropy, *J. geophys. Res.*, **105**, 7893–7908.
- Tyburczy, J.A. & Waff, H.S., 1983. Electrical conductivity of molten basalt and andesite to 25 kilobars pressure: geophysical significance and implications for charge transport and melt structure, *J. geophys. Res.*, **88**, 2413–2430.
- Wang, L., Zhang, Y. & Essene, E., 1996. Diffusion of the hydrous component in pyrope, *Am. Mineral.*, **81**, 706–718.
- Wenk, H.-R., Bennet, K., Canova, G.R. & Molinari, A., 1991. Modelling plastic deformation of peridotite with the self-consistent theory, *J. geophys. Res.*, **96**, 8337–8349.
- Woods, S.C., Mackwell, S. & Dyar, D., 2000. Hydrogen in diopside: diffusion profiles, *Am. Mineral.*, **85**, 480–487.
- Xu, Y. & Shankland, T.J., 1999. Electrical conductivity of orthopyroxene and its high pressure phases, *Geophys. Res. Lett.*, **26**, 2645–2648.
- Xu, Y., Poe, B.T., Shankland, T.J. & Rubie, D.C., 1998. Electrical conductivity of olivine, wadsleyite, and ringwoodite under upper-mantle conditions, *Science*, **280**, 1415–1418.
- Xu, Y., Shankland, T.J. & Poe, B.T., 2000. Laboratory-based electrical conductivity in the Earth's mantle, *J. geophys. Res.*, **105**, 27 865–27 875.
- Zhang, S. & Karato, S.-I., 1995. Lattice preferred orientation of olivine aggregates deformed in simple shear, *Nature*, **375**, 774–777.